JOURNAL OF GUIDANCE, CONTROL, AND DYNAMICS
Vol. 30, No. 2, March–April 2007

Modeling and Near-Space Stationkeeping Control of a Large High-Altitude Airship

David K. Schmidt*
University of Colorado, Colorado Springs, Colorado 80918

DOI: 10.2514/1.24865

A key technical challenge for high-altitude, or near-space, concepts is autonomous stationkeeping: the ability to remain fixed over a geolocation in the presence of winds. Although operational altitudes of 65,000 ft and above are above weather (i.e., storms, rain), winds are still present. To stationkeep in the presence of these winds requires propulsive power, and these vehicles tend to be quite power-limited. This paper focuses on the analysis of the stationkeeping performance of a large notional airship operating at an altitude of 65,000 ft, with a focus on the maneuvering power required. The vehicle has a lifting-gas volume of 6.1×10^6 ft^3 and is solar electric powered, with the entire upper surface covered by solar cells. Electric motors and propellers provide propulsion, and batteries are used for power storage. In this paper, the vehicle's surge and directional dynamics are characterized, the wind environment is modeled, and simple control and guidance algorithms are developed and evaluated. In particular, the maneuvering power required is statistically determined, using a covariance analysis. It is shown that the vehicle is dynamically stable and sluggish, and that significant thrust and control power may be required to stationkeep in turbulence. This additional maneuvering power required may be a significant design driver.

Nomenclature

A	=	reference area for aerodynamic coefficients
C_D	=	aerodynamic drag coefficient
I_z	=	vehicle yaw inertia
$L_{()}$	=	characteristic lengths in gust model
L/D	=	airship length-to-diameter ratio
l	=	reference length for aerodynamic coefficients
m	=	vehicle mass
N	=	aerodynamic yawing moment on vehicle
r	=	vehicle perturbation yaw velocity
t	=	perturbation thrust
U	=	vehicle velocity relative to air mass x_{body} component
u	=	vehicle perturbation velocity relative to air mass x_{body} component
u_g	=	gust velocity x_{body} component
V	=	vehicle velocity relative to air mass y_{body} component
v	=	vehicle perturbation velocity relative to air mass y_{body} component
v_g	=	gust velocity y_{body} component
$\boldsymbol{V}_{\text{Inertial}}$	=	vehicle inertial-velocity vector
$\boldsymbol{V}_{\text{Relative}}$	=	vehicle velocity vector relative to the moving air mass
$\boldsymbol{V}_{\text{Wind}}$	=	steady air mass or wind velocity vector
V_{Wind}	=	wind velocity magnitude
$V_{\text{Wind-50\%}}$	=	50th percentile (mean) wind velocity
$V_{\text{Wind-95\%}}$	=	95th percentile wind velocity
$V_{\text{Wind-99\%}}$	=	99th percentile wind velocity
W_{OEW}	=	airship operating empty weight (lifting gas not included)
$\dot{X}$	=	inertial vehicle velocity component X inertial direction
XX	=	aerodynamic plus thrust force on vehicle x_{body} component
x_{body}	=	body-fixed reference frame; axial direction
$\dot{Y}$	=	inertial vehicle velocity component Y inertial direction
YY	=	aerodynamic force on vehicle y_{body} component
y_{body}	=	body-fixed reference frame, lateral direction
δ_r	=	perturbation rudder deflection
ρ	=	atmospheric density
$\sigma_{()}$	=	gust intensity
$\Phi_{()}$	=	gust power spectrum
ψ	=	vehicle body heading angle
$\boldsymbol{\omega}$	=	vehicle's angular velocity vector, inertial or relative
$()_0$	=	reference or equilibrium value of the quantity ( )

Introduction

THERE is growing worldwide interest in a new concept consisting of using autonomous atmospheric flight vehicles as platforms operating for extended periods of time at very high altitudes (between 65,000 and 300,000 ft) to accomplish military and commercial missions heretofore accomplished using spacecraft (cf. [1]). Such missions include persistent ground surveillance and/or communications, for example. In the U.S. defense community, and increasingly in the commercial world, using such vehicles in this manner is referred to as a near-space solution to a mission requirement, as opposed to a space-based solution. And the platforms are referred to as near-space vehicles.

Currently, few vehicles operate in this altitude range, and when they do, it is for a relatively brief time. But interest in near-space solutions is increasing because such solutions are potentially less expensive and more flexible than space-based solutions. Plus, near-space solutions offer the possibility of continuous coverage over the ground target area—the near-space vehicle can remain fixed over a target, but a spacecraft can only pass over that location once each orbit. Some missions call for the near-space platform to remain aloft for up to 1 yr.

Interest in near-space solutions has also increased because they are more feasible than in the past, due to technological advances in lightweight materials and in solar power technology. Many near-space vehicular concepts would use some form of solar-electric power for propulsion—electric motors and propellers, for example. Near-space vehicle concepts may be heavier that air (unmanned air vehicles, or UAVs), lighter than air (airships), or hybrid designs that

Presented as Paper 6781 at the Guidance, Navigation, and Control Conference, Keystone, CO, 21–24 August 2006; received 28 April 2006; accepted for publication 17 August 2006.

*Professor Emeritus, Department of Mechanical and Aerospace Engineering, Space and Near-Space Research Group, 1420 Austin Bluffs Parkway. Fellow AIAA.

both generate aerodynamic lift and possess buoyancy. But no near-space vehicle has delivered the capability of remaining aloft for a year, and all are severely power limited.

A key technical challenge is autonomous stationkeeping, or the ability to remain fixed over a specified geolocation in the presence of winds. Although near-space altitudes of 65,000–300,000 ft are above weather (i.e., storms, rain), winds still exist. And to stationkeep in the presence of these winds requires propulsive power. This paper focuses on the analysis of stationkeeping of a notional large solar powered airship operating at an altitude around 65,000 ft, with particular interest in the additional propulsive power required to stationkeep in atmospheric turbulence.

Because near space is a new concept, published works on the dynamic analysis and control of very large, solar powered, autonomous airships at high altitude are sparce in the open literature to date. (The author is aware of work currently under way in industry, but has been unable to find anything reporting on this work in the open literature.) Hence the main intended contributions of this work are to use fairly conventional systems-analysis techniques to gain insight into the dynamic characteristics of these novel vehicles in this unusual flight condition, and to assess the control power requirements. Such required control power will only diminish the limited excess onboard power available.

An autonomous solar power vehicle was the subject of study at the University of Stuttgart ([2–4]), and in-flight experience was gained. But the vehicle was quite small (51 ft in length) and only low-altitude flight was considered. It is interesting to note, however, the difficulties caused by atmospheric turbulence with regard to the control of this vehicle ([2]), which is a key aspect of this investigation.

A large, high-altitude, autonomous vehicle was described in [5], and scaled versions of the vehicle have been built and flown ([6]). But as with the Stuttgart study, the scaled versions are quite small (60 ft in length) and have been only flown at low altitude. And again, difficulties of control in turbulence were significant, as noted in [6].

A much larger airship, 460 ft in length, was the subject of study in [7]. But this vehicle was manually controlled, and again only low-altitude flight was the focus. However, [7] provides much of the basis for the aerodynamic characterization of the vehicle in this current investigation, because the vehicles are of similar size.

In the remaining sections of the paper, the flight-dynamics model of the airship will be developed, stationkeeping guidance-and-control laws synthesized, and the wind environment characterized. Then using these results, a stochastic covariance analysis will be performed to determine the additional control power (thrust and fin deflection) required to maintain position in the presence of the atmospheric turbulence.

Notional Airship

The vehicle configuration investigated is a large airship with characteristics described in Fig. 1. Though notional, this vehicle has many characteristics similar to vehicles currently being considered for near-space applications. To carry some of the larger payloads (e.g., surveillance and/or communication equipment and associated electronics) to 65,000 ft requires a large airship. Lifting-gas volume is over 6 million ft^3, and the vehicle is neutrally buoyant at the 65,000-ft altitude. The operational empty weight, W_{OEW}, (gas envelope) volume, and length-to-max-diameter ratio, L/D, were all selected based on empirical airship-design data from [8]. The vehicle would be entirely solar-electric powered, with the upper surface covered by solar cells. Electric motors and propellers would provide propulsion. Additional onboard power will be required for the payload and auxiliary equipment, and batteries would be used for power storage. No additional power generation capability is assumed.

Flight-Dynamics Modeling

In this study the focus is on the motion of the neutrally buoyant airship in a horizontal plane at 65,000-ft altitude. Motion in the vertical plane could be considered as well, but due to the geometry of the airship and the characteristics of the atmospheric turbulence, the vehicle's motion in the horizontal plane was considered the most critical at this point. Further, the focus will be on three critical degrees of freedom of the vehicle, forward or surge position, lateral position, and yawing rotation. The rolling degree of freedom, or "pendulum mode" dominated by the vehicle's mass properties, will be ignored in this study, as this degree of freedom is assumed to contribute little in terms of the dynamics governing the vehicle's inertial position. As shown in [8], for example, the rolling pendulum mode is typically only very lightly coupled to the lateral-translation and yawing modes, and therefore contributes little to the vehicle's lateral translation. So a simple roll damper should adequately damp that ignored roll mode.

Using small-perturbation theory, the motion of the vehicle is decomposed into two components, the equilibrium flight condition, and the deviations from that flight condition. For stationkeeping in turbulence, the equilibrium condition is defined as the vehicle remaining stationary in inertial space, pointed into a steady wind, and thrusting to maintain that fixed position. So this equilibrium position is taken to be a fixed inertial position at 65,000-ft altitude, with the vehicle maintained in that position in the presence of a steady wind.

Now let the inertial velocity (vector) of the vehicle $\boldsymbol{V}_{\mathbf{Inertial}}$ be defined in terms of the motion of the vehicle *relative to the steady moving air mass*, plus the constant velocity of that air mass relative to the ground. That is, let

$$\boldsymbol{V}_{\mathbf{Inertial}} = \boldsymbol{V}_{\mathbf{Wind}} + \boldsymbol{V}_{\mathbf{Relative}} \tag{1}$$

Likewise, let the vehicle's angular velocity $\boldsymbol{\omega}_{\mathbf{Inertial}}$ be similarly defined, or

$$\boldsymbol{\omega}_{\mathbf{Inertial}} = \boldsymbol{\omega}_{\mathbf{Wind}} + \boldsymbol{\omega}_{\mathbf{Relative}} \tag{2}$$

and here, $\boldsymbol{\omega}_{\mathbf{Wind}} = 0$.

Now let $\boldsymbol{V}_{\mathbf{Relative}}$ have surge and lateral components U and V in the vehicle's body-fixed coordinate frame, and let U and V be expressed in terms of the equilibrium flight condition plus perturbations from that equilibrium condition. Or

$$U = U_0 + u \qquad V = V_0 + v \tag{3}$$

Vehicle Characteristics:

Volume = 6.1x10^6 ft^3
Length = 450 ft
Width = 100 ft
W_{OEW} = 30,000 lb
Solar electric powered
Propeller driven
Payload power = 3 kW (HAA)

Performance Requirements:

Operating altitude - 65,000 ft
Endurance at altitude ~ 1 year
Stationkeeping capability in wind

Fig. 1 Notional airship considered.

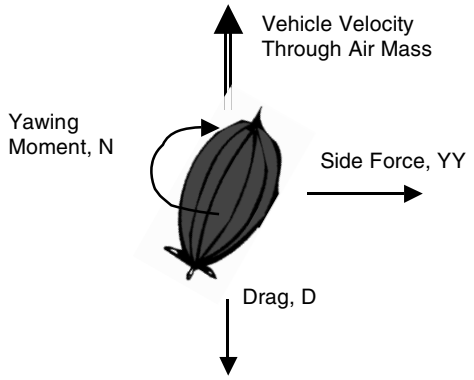

Fig. 2 Force and moment schematic.

Note that because the equilibrium condition is stationkeeping heading directly into the steady wind, $U_0 = V_{\text{Wind}}$. and $V_0 = 0$.

The motion associated with the perturbations from the equilibrium flight condition is governed by three familiar linear differential equations (cf. [8]), each associated with one of the 3 degrees of freedom.

$$m\dot{u} = XX \qquad m[\dot{v} + (U_0 - V_{\text{Wind}})r] = YY \qquad I_z\dot{r} = N \tag{4}$$

In these equations, u, v, and r are perturbations from equilibrium, with u the forward (body axis) component of the vehicle's velocity relative to the steady moving air mass, v the lateral (body axis) component of the vehicle's relative velocity, and r the vehicle's relative yaw rate. However, because the equilibrium flight condition involves stationkeeping at a *fixed* inertial position, u, v, and r are also inertial velocities. Also note that U_0 is equal and opposite to V_{Wind}, so the equilibrium inertial velocity is $U_0 - V_{\text{Wind}} = 0$.

Further in the preceding equations, YY is the aerodynamic side force, N is the aerodynamic yawing moment, and the force XX includes both the aerodynamic drag D and the propulsive thrust. The aerodynamic forces and moment are shown schematically in Fig. 2.

Finally, m is the vehicle mass and I_z is the vehicle inertia about its yaw axis. For our notional vehicle, the gross weight is 34,810 lb and so $m = 1081$ slug. The value for I_z was derived from [7]. The inertia in the reference was scaled proportionally to the masses of the notional vehicle and the vehicle in [7]. The resulting value for the notional vehicle's inertia is $I_z = 1.91 \times 10^7$ slug $\cdot$ ft^2.

The forces and moment on the airship due to its motion relative to the air mass are expressed in terms of aerodynamic coefficients, dynamic pressure, a selected reference area, and a selected reference length. Using fairly standard notation in atmospheric flight mechanics (again, cf. [8]), the surge and side forces and yawing moment are expressed, respectively, as

$$\begin{aligned} XX &= X_u u_A + X_\delta \delta_r + X_t t \\ YY &= Y_v v_A + Y_r r + Y_{\dot{v}}\dot{v} + Y_{\dot{r}}\dot{r} + Y_\delta \delta_r \\ N &= N_v v_A + N_r r + N_{\dot{v}}\dot{v} + N_{\dot{r}}\dot{r} + N_\delta \delta_r \end{aligned} \tag{5}$$

where

$$u_A = u + u_g \qquad v_A = v + v_g$$

The coefficients $X_{(\cdot)}$, $Y_{(\cdot)}$, and $N_{(\cdot)}$ in the preceding expressions are defined in Table 1. Many of these coefficients are expressed as functions of the dynamic pressure q, where

$$q = 1/2\rho U_0^2 \tag{6}$$

Here ρ is taken to be the standard atmospheric density at 65,000 ft and U_0 is the steady wind velocity V_{Wind}.

Several coefficients are also functions of a selected reference area and a reference length. To be consistent with the data in [7], the reference area for the directional coefficients (not the surge) is

$$A = (Vol)^{2/3} \tag{7}$$

and the characteristic length is the cube root of the gas volume, or

$$l = (Vol)^{1/3} \tag{8}$$

Finally, the coefficients associated with the apparent masses (discussed further, next) are also shown.

To complete this model for forces and yawing moment, the stability derivatives must be estimated. As discussed in [9], C_D (the trim drag coefficient) is taken to be 0.120 (referred to maximum cross-sectional area) for this vehicle. Also, C_{X_δ} is taken to be zero and X_t is unity. The values chosen for the remaining stability derivatives listed in Table 1 were again based on those in [7], because the vehicle in this reference has size and geometry similar to our study vehicle. But the vehicle in [7] exhibited reduced static stability due a reduction of the stabilizing fin size by 40%. So the stability derivatives taken from [7] were adjusted for this fact.

The effectiveness of the aft stabilizing fins was parametrically increased, and the stability derivatives associated with side force and yawing moment (listed in Table 2) have been adjusted accordingly. In particular, C_{Y_r} and all three $C_{N_{(\cdot)}}$ derivatives were assumed to be proportional to tail effectiveness, which is typically the case for conventional aircraft (ignoring the wing). The remaining two derivatives were not adjusted from their values in [7].

The remaining aspects of the model described in Table 1 are the apparent masses. Apparent-mass effects arise from the force on an accelerating vehicle associated with the concomitant acceleration of the air particles being displaced by the vehicle's accelerating motion. (Note that apparent-mass effects are typically significant for airships, but are frequently ignored when analyzing heavier-than-air vehicles, or aircraft) The values selected for four of the apparent masses in this model were based on those of [7], because the length and width of the two vehicles are similar. However, the apparent masses in [7] were scaled proportional to the ratio of the atmospheric density at 65,000 ft and the density at sea level. The resulting masses are listed in Table 3. The apparent mass associated with the surge (u) degree of freedom was taken to be zero. Based on the geometry of the vehicle, this apparent mass would be significantly less that the other four. Plus, [7] provided no information on this characteristic.

Table 1 Definition of force and moment coefficients

Coefficient	Definition	Coefficient	Definition	Coefficient	Definition
X_u	$-(2C_D/U_0)qA$	Y_v	$C_{Y_v}qA$	N_v	$C_{N_v}qAl$
		Y_r	$C_{Y_r}qA$	N_r	$C_{N_r}qAl$
		$Y_{\dot{v}}$	Apparent Y_v mass	$N_{\dot{v}}$	Apparent N_v mass
		$Y_{\dot{r}}$	Apparent Y_r mass	$N_{\dot{r}}$	Apparent N_r mass
X_δ	$C_{x_\delta}qA$	Y_δ	$C_{Y_\delta}qA$	N_δ	$C_{N_\delta}qAl$

Table 2 Values for stability derivatives

Stability derivative	Value	Stability derivative	Value
C_{Y_v}	-9.5×10^{-3} (per fps)	C_{N_v}	$-.021$ (per fps)
C_{Y_r}	267/Vel (per rad/s)	C_{N_r}	-438/Vel (per rad/s)
C_{Y_δ}	0 (per rad)	C_{N_δ}	$-.358$ (per rad)

Table 3 Values for apparent masses selected in the model

Apparent mass	Value	Apparent mass	Value
Apparent Y_v mass	-471 slug	Apparent N_v mass	3814 slug · ft^2
Apparent Y_r mass	3814 slug · ft^2	Apparent N_r mass	-3.51×10^6 slug · ft^2

Table 4 Transfer functions for the notional vehicle's dynamics

Degree of freedom	Transfer functions from thrust t, lb	Transfer functions from rudder δ_r, rad
u, fps	$\frac{0.000925(s+0.261)(s+0.527)}{(s+0.261)(s+0.0156)(s+0.527)}$	0
v, fps	0	$\frac{-0.0958(s+13.9)(s+0.0156)}{(s+0.261)(s+0.0156)(s+0.527)}$
r, rad/s	0	$\frac{-0.0390(s+0.0824)(s+0.0156)}{(s+0.261)(s+0.0156)(s+0.527)}$

Table 5 Guidance-and-control logic

Error	Attitude logic	Error	Attitude logic
$\varepsilon_{\dot{X}} = \dot{X}_{\text{command}} - \dot{X}$	$t = K_{\dot{X}}(\varepsilon_{\dot{X}} + 0.01 \int \varepsilon_{\dot{X}} dt)$	$\varepsilon_X = X_{\text{command}} - X$	$\dot{X}_{\text{command}} = K_X \varepsilon_X$
$\varepsilon_{\dot{Y}} = \dot{Y}_{\text{command}} - \dot{Y}$	$\delta_r = K_{\dot{Y}} \varepsilon_{\dot{Y}}$	$\varepsilon_Y = Y_{\text{command}} - Y$	$\dot{Y}_{\text{command}} = K_Y \varepsilon_Y$

Based on the equations of motion given previously and the numerical values for the parameters in the model as described, the small-perturbation dynamics of the vehicle may be described in terms of the transfer functions given in Table 4.

It is noted that the dynamics are decoupled and stable. The decoupling arises because the drag associated with control-fin deflections are zero for he chosen reference condition. The characteristic modes of the vehicle are also apparent. In particular, the surge dynamics are dominated by a surge mode with a pole at -0.0156/s. The directional dynamics are dominated by a yaw mode with a pole at -0.527/s and a sideslip mode dominated by a pole at -0.261/s. All these characteristics are fairly similar to conventional low-altitude airships.

Now to be addressed are the kinematics. As noted previously, u and v are the components of the vehicle's inertial velocity in the forward and lateral directions, respectively, referenced to a body-fixed coordinate frame. Let $\dot{X}$ and $\dot{Y}$ be the components of the vehicle's inertial velocity referenced to an inertial reference frame, where $\dot{X}$ is directed into the steady wind for stationkeeping. Then, noting that reference lateral velocity V_0 and heading ψ_0 are both zero, the kinematics are defined by the following relations.

$$\begin{aligned} \dot{X} &= (U_0 + u)\cos\psi - v\sin\psi - V_{\text{wind}} \\ \dot{Y} &= (U_0 + u)\sin\psi + v\cos\psi \qquad \dot{\psi} = r \end{aligned} \tag{9}$$

Here, ψ is the inertial heading of the vehicle (not its velocity heading) or the inertial direction in which the vehicle is pointing. If ψ is assumed small (<15 deg), the preceding equations may be linearized to yield the following.

$$\dot{X}_{\text{perturbation}} = (U_0 + u) - V_{\text{Wind}} = u \qquad \dot{Y}_{\text{perturbation}} = U_0\psi + v \tag{10}$$

This kinematics model, plus the dynamic model summarized in Table 5, completes the development of the flight-dynamic model.

Stationkeeping Guidance-and-Control Logic

The stationkeeping objective, depicted schematically in Fig. 3, is to keep position error small in the presence of atmospheric turbulence. This objective may be met by using a multiloop guidance-and-control feedback system with block diagram, depicted in Fig. 4.

The block labeled "Vehicle Dynamics" represents the vehicle, as modeled previously. The "Attitude Controller" block represents inner-loop attitude-control logic. This inner loop is designed to drive $\dot{X}$ and $\dot{Y}$ to match the commanded inertial velocities, using t and δ_r as control inputs. The "Guidance Algorithm" block is the outer-loop controller. This guidance algorithm generates the required inertial-

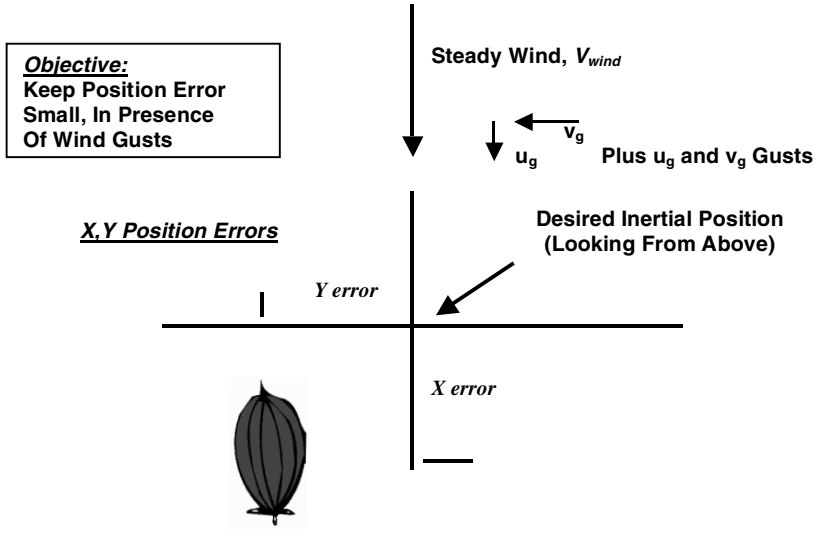

Fig. 3 Stationkeeping in turbulence.

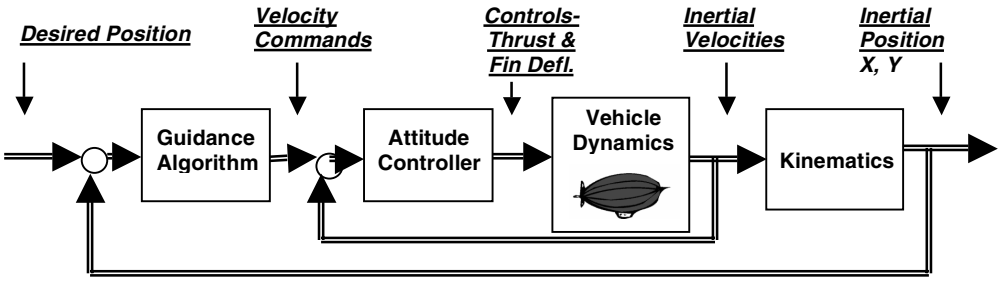

Fig. 4 Guidance-and-control system block diagram.

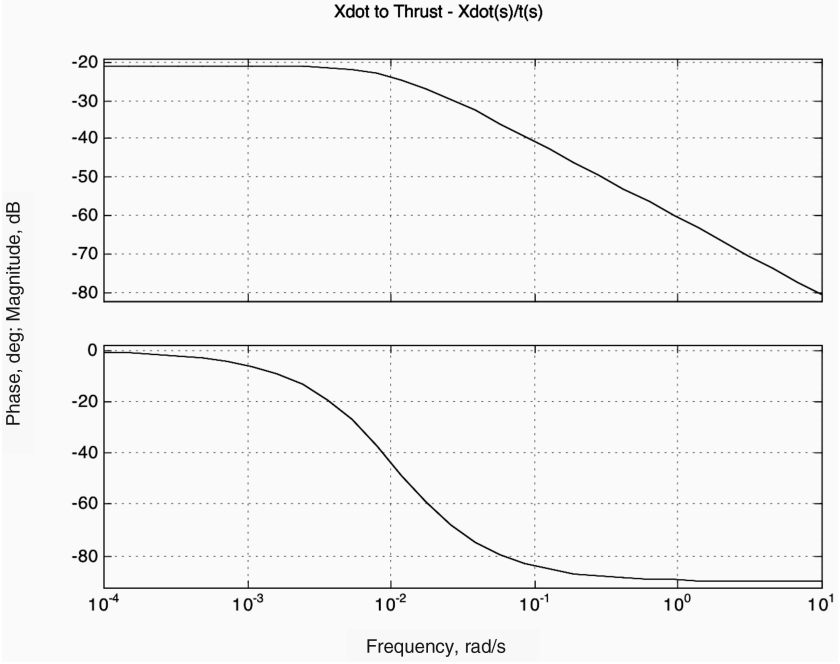

Fig. 5 Open-loop bode plot of inertial velocity $\dot{X}$ to thrust, fps/lb.

velocity commands to the inner loop in order to drive the inertial position to the desired inertial position. Finally, measurements of the inertial position and inertial velocities could be obtained from an onboard GPS, for example.

Referring to the vehicle dynamics developed previously, the inner- and outer-loop control laws may be synthesized using loop-shaping as follows. Shown in Figs. 5 and 6 are the open-loop Bode plots of the inner-loop dynamics, namely, $\dot{X}/t(s)$ and $\dot{Y}/\delta_r(s)$.

For inner-loop $\dot{X}$ control, Fig. 5 suggests a proportional-plus-integral (PI) controller with a compensator zero at about $0.01/\text{s}$ would yield an open-loop transfer of approximately ω_c/s, and the compensator gain $K_{\dot{X}}$ ($\approx\omega_c/0.000925$ in this loop) in Table 5 selected to yield the desired crossover frequency. For inner-loop $\dot{Y}$ control, Fig. 6 indicates that the open-loop transfer would be approximately ω_c/s with only pure gain compensation. So $K_{\dot{Y}}$ ($\approx\omega_c$ in this loop) may be selected to yield the desired crossover frequency in this loop. Such control laws lead to excellent stability robustness.

With these inner-loop controllers in place, the $\dot{X}$ and $\dot{Y}$ velocities will follow their commanded velocities, and so the outer-loop controllers need only be pure gains K_X and K_Y, selected to yield the desired crossover frequencies in these outer loops.

The control logic developed for these attitude controller and guidance algorithms is summarized in Table 5. All gain parameters $K_{(\cdot)}$ were chosen to provide sufficient frequency separation (at least a factor of five) between the inner and outer loops, consistent with conventional feedback-systems theory. Finally, the $\dot{X}$ and $\dot{Y}$ inner-loop crossover frequencies were selected to be equal (for example, 0.1 rad/s), as were the X and Y outer-loop crossover frequencies (for example, 0.02 rad/s). Keeping a balanced bandwidth tends to yield optimum stationkeeping performance, but could be adjusted if control power limitations were present.

To demonstrate the performance of the preceding guidance-and-control system, simulated system time responses are shown in Fig. 7. In this simulation, the vehicle is assumed to be thrusting into a steady 40 kn headwind, and the feedback systems must drive the initial position error to zero to achieve the desired stationkeeping position. The selected initial position error is $X_0 = -50$ ft, $Y_0 = 50$ ft, and the desired final position (X and $Y = 0$) is reached in approximately 1.5 minutes, with the vehicle decelerating as it approaches this final position. The time histories of all system responses, including the control inputs perturbation thrust and rudder deflection are shown in the figure. It is also noted that the initial perturbation thrust is about 100 lb, and the initial rudder deflection is about 6 deg.

Recall that in the flight condition being considered, the vehicle is both thrusting into a steady 40-kn headwind and the thrust and rudder are being modulated to maneuver the vehicle to achieve the desired stationkeeping position. The time histories shown in the previous figure are the perturbations in thrust, surge velocity, etc., necessary to accomplish this maneuvering.

It is significant that the heading angle deviates only slightly from zero, which indicates that the vehicle is "crabbing," because it essentially points into the steady wind as it maneuvers toward the desired final position. If the vehicle's inertial X, Y position was plotted, the vehicle's trajectory would be essentially a straight line. It is also noted that all responses are smooth and stable. This guidance scheme that points the vehicle into the wind will tend to lead to the minimum time required to maneuver to the desired stationkeeping location in a uniform wind field.

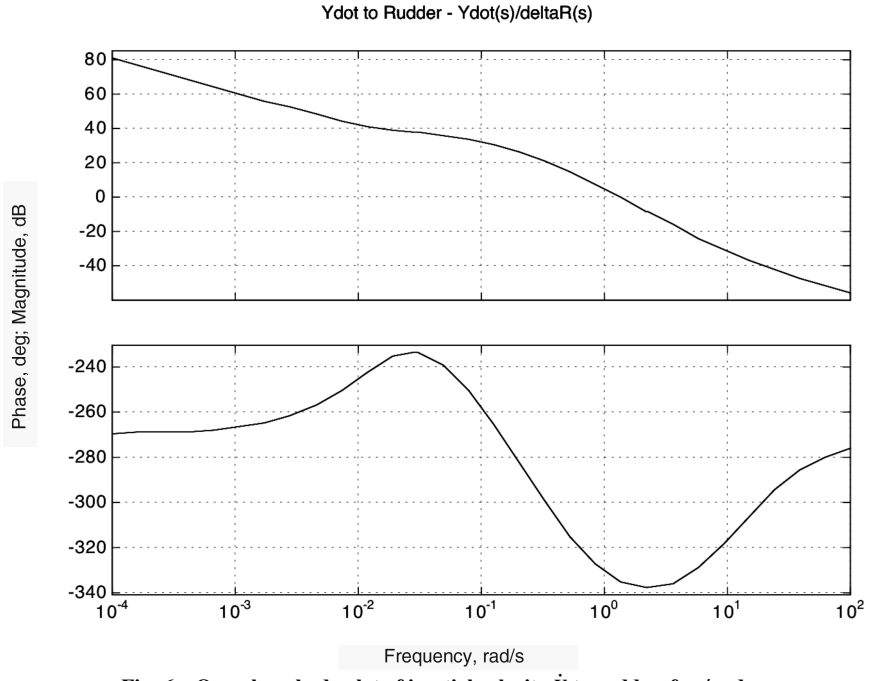

Fig. 6 Open-loop bode plot of inertial velocity $\dot{Y}$ to rudder, fps/rad.

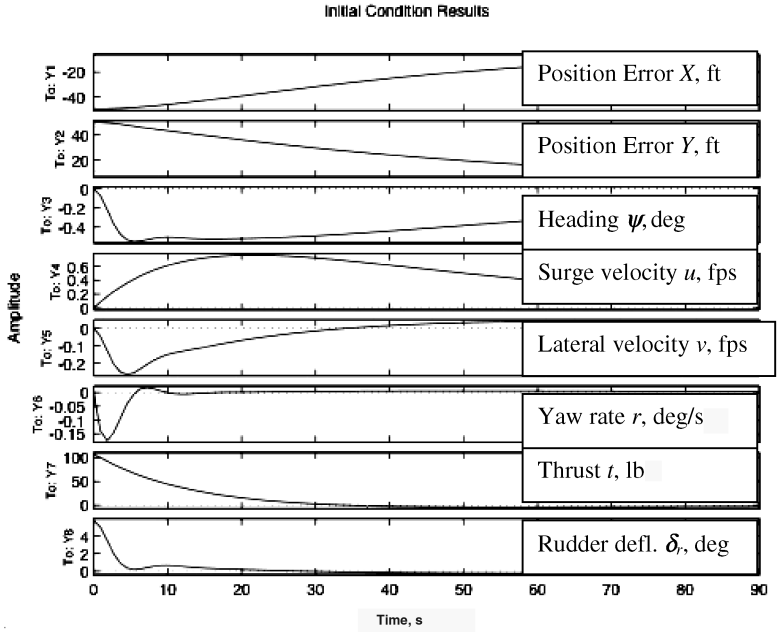

Fig. 7 Closed-loop system time histories.

Wind Environment

Key aspects of the wind environment may be characterized statistically, using data from the National Weather Service (cf. [10]). An example scatter diagram (taken from [9]) of wind velocity as a function of altitude over Akron, Ohio for the year 2004 is shown in Fig. 8. Akron was one of several sites investigated, with sites selected due to their latitudes and weather patterns and because they are locations where airship testing might be expected to occur. Although the wind data reveals a lower-wind "knee" around 70,000 ft, it is clear that wind speed as high as 100 kn exist at this altitude. Using this data, the wind statistics for each month during 2004 may be extracted, and relevant statistics are summarized in Table 6. Based on these wind statistics, a steady wind of 40 kn was assumed in this analysis. This velocity (40 kn) was representative of the higher mean winds in the winter months in the geolocations considered. So stationkeeping over a fixed geolocation involves flying at 40 knots into that steady headwind.

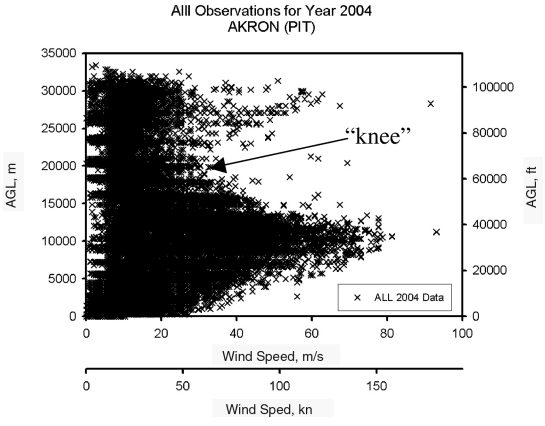

Fig. 8 Wind velocities over Akron, Ohio in 2004.

Table 6 Winds over Akron, Ohio at 65,000 ft in 2004 at 50th, 95th, and 99th percentile.

Month	Obs.	V_{Wind} 50%, kn	V_{Wind} 95%, kn	V_{Wind} 99%, kn
January	118	26.1	41.8	48.6
February	133	26.0	47.0	56.4
March	179	19.7	36.9	44.7
April	163	12.7	21.5	25.3
May	162	9.7	20.0	25.5
June	170	9.5	18.0	21.5
July	155	12.6	19.0	21.5
August	172	9.8	18.0	21.0
September	155	9.2	18.5	23.3
October	168	13.0	22.0	26.0
November	173	22.1	38.0	45.0
December	132	34.4	68.5	85.6

A statistical turbulence model, the Dryden gust model as documented in [11], is depicted in Fig. 9 along with the spectrum models (equations) given next. This figure shows the likelihoods of the (rms) intensity of the gust velocity as a function of altitude. Analysis of this data indicates that at the higher altitudes in which we are interested, the gust intensity associated with severe turbulence will be be about 8 ft/s (rms). And the probability of exceeding severe turbulence at 65,000 ft is 1×10^{-5}.

The gust frequency spectra are described in terms of the following power-spectral densities.

$$\Phi_{u_g}(\omega) = \sigma_u^2(2L_u/\pi U_0)\left[\frac{1}{1+(L_u\omega/U_0)^2}\right] \quad \text{and}$$
$$\Phi_{v_g}(\omega) = \sigma_v^2(L_v/\pi U_0)\left[\frac{1+3(L_v\omega/U_0)^2}{[1+(L_v\omega/U_0)^2]^2}\right] \tag{11}$$

Here, u_g and v_g are the surge and lateral gust velocities, respectively, and σ_u and σ_v are the rms intensities of the u_g and v_g gust velocities, respectively, obtained from Fig. 9. U_0 is the reference velocity of the flight vehicle (airship) into the steady wind (which, as noted previously, is taken to be 40 kn). And finally, at the altitudes being considered in this study, the characteristic lengths $L_u = L_v = 1750$ ft.

Note that although the turbulence intensity diminishes with altitude, it is not zero.

Maneuvering Power Required

With the vehicle-dynamic model and guidance-and-control logic now developed, as well as a statistical wind model, it is possible to assess the control power required for maneuvering in turbulence. The analysis technique is a covariance analysis, as presented in [12,13], for example. This analysis is performed using the preceding linear

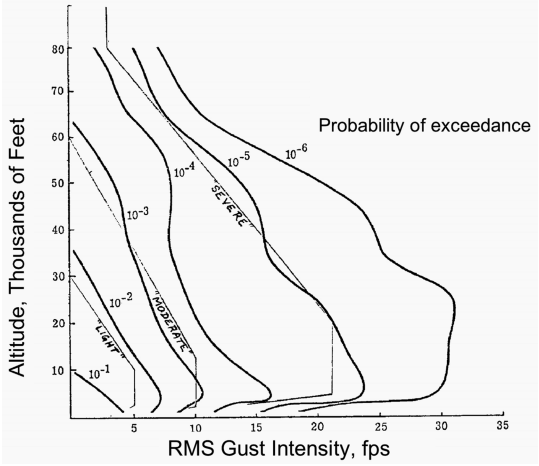

Fig. 9 Statistical turbulence model; gust intensity [11].

models of the vehicle dynamics, control loops, and turbulence spectra, and the Lyapunov equation associated with this closed-loop stochastic system is solved to yield the covariances of the system's responses and control inputs.

The results from such a statistical analysis are shown in Figs. 10 and 11. Plotted in these figures are the standard deviations of the vehicle's inertial position errors vs the standard deviations of the control inputs (perturbation thrust and rudder deflection) necessary to maintain position in the presence of severe turbulence.

To generate these results, the compensator gains in the guidance-and-control logic given in Table 5 were adjusted parametrically, resulting in a family of guidance-and-control system designs with only the (inner- and outer-loop) gain-crossover frequencies being varied. This parametric set of designs ranges from a high-performance design to a low-performance design, with two intermediate designs.

As the point designs transition from lower to higher performance, the rms control usage (thrust and rudder deflection) increases and the rms position error is reduced. Arrows in the figures show a specific example. To maintain an rms longitudinal X position error of less than 2 km (~6500 ft) in the presence of turbulence requires an rms thrust level of at least 5 lb. Additionally, maintaining an rms lateral Y position error of less than 2 km requires an rms rudder deflection of at least 5 deg.

Both the required rudder deflection and the thrust required are significant. As shown in [9], a key performance metric for these large solar powered airships is the onboard power available compared with the power required for stationkeeping. And the excess power available is quite limited. The thrust required for this vehicle just to maintain a fixed position (at 65,000 ft) in a *constant* 40-kn wind is about 380 lb. Hence, the 5-lb (rms) *additional* thrust requirement to

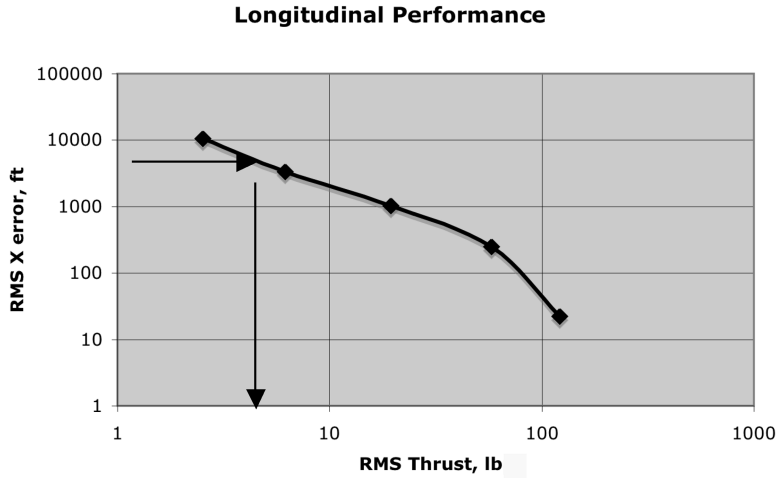

Fig. 10 Longitudinal stationkeeping performance.

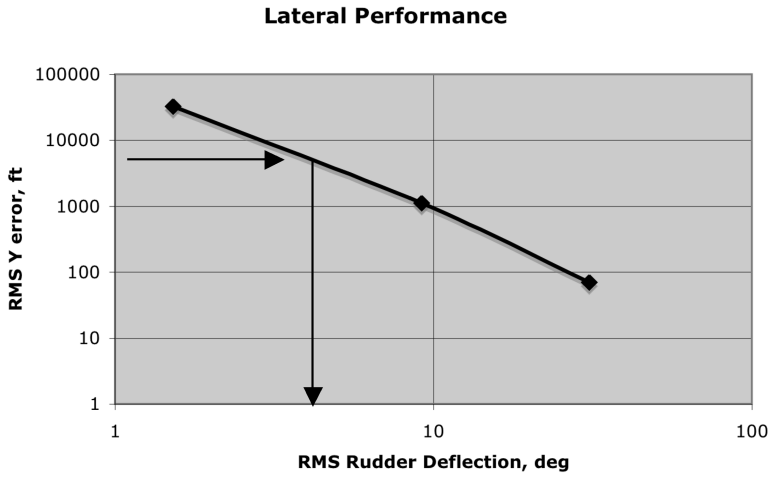

Fig. 11 Lateral stationkeeping performance.

remain within 2 km of the desired position in severe turbulence represents only a 1.4% increase in power required. But if it is required to stationkeep within 1000 ft of a desired location, for example, the additional thrust required increases to about 20 lb, rms. This additional power could be an important consideration in the vehicle's design and its operational capability. Finally, the gust intensities shown in Fig. 9 indicate that the greater turbulence at low altitude (5000 to 10,000 ft) may create control challenges as the vehicle transitions to and from its operating altitude.

Conclusions

Presented was the development of a model for the flight dynamics of a large airship operating at 65,000-ft altitude and the synthesis of a guidance-and-control system for stationkeeping in the presence of the winds at that altitude. The model included the surge and lateral-directional degrees of freedom of the vehicle, and it was determined that the dynamics were stable and sluggish, dominated by three nonoscillatory modes. These characteristics are similar to those of smaller conventional airships operating at much lower altitudes.

The development of the guidance-and-control laws followed a conventional loop-shaping approach compatible with the characteristic dynamics of the vehicle. The methodology exploited the natural frequency separation between the vehicle's attitude and position dynamics, and the resulting control and guidance laws were very simple, The loop-shaping approach used yields robust stability margins in all loops, and the closed-loop responses are natural and well-behaved.

A stochastic analysis of the resulting closed-loop system assessed the control power required to maintain desired position in the presence of turbulence. It was noted that severe turbulence intensity at the operating altitude corresponds to a gust intensity of around 8 fps. For this level of turbulence, approximately 5 lb (rms) of thrust will be required to keep the rms longitudinal position error within 2 km, and 5-deg (rms) rudder deflection is required to keep lateral position error below 2 km. This control power requirement can increases the total power required for stationkeeping in winds, a key design parameter for these vehicles.

Acknowledgments

This research was partially funded by the U.S. Army Space and Missile Defense Battle Laboratory in Colorado Springs, Colorado. Stew Stout was the technical monitor. This support is appreciated. The author would also like to acknowledge the many helpful suggestions of the reviewers, which improved the quality and clarity of the paper.

References

[1] Stevens, H., "Near Space," *Air Force Magazine*, Vol. 88, No. 7, 2005; also available at www.afa.org/magazine/July2005/0705near.asp.

[2] Kroplin, B., and Schafer, I., "Experiences by Design and Operation of the Solar Powered Airships Lotte 1-3," 11th AIAA Lighter than Air Systems Conference, Clearwater, FL, AIAA Paper No. 95-1613-CP, 1995.

[3] Kaempf, B. G., and Well, K. H., "Attitude Control System for a Remotely-Controlled Airship," 11th AIAA Lighter than Air Systems Conference, Clearwater, FL, AIAA Paper No. 95-1622-CP, 1995.

[4] Wimmer, D.-A., Bildstein, M., Well, K.H., Schlenker, M., Kingl, P., and Kröplin, B.-H., "Research Airship 'Lotte': Development and Operation of Controllers for Autonomous Flight Phases," *2002 IEEE/RSJ International Conference on Intelligent Robots and Systems*, Inst. of Electrical and Electronics Engineers, Piscataway, NJ, 2002.

[5] Onda, M., "Stratospheric Unmanned Airship for Power Generating Plants," *12th ISAS Space Energy Symposium*, Inst. of Space and Astronomical Sciences, Sagamihara, Japan, 1993.

[6] Onda, M., Misawa, M., Fujita, M., Fujino, Y., Kaya, N., Tomita, K., Yamada, M., Maizumi, O., and Sasuga, M., "A Ground-to-Airship Microwave Transmission Test Plan for Stationary Aerial Platform," 11th AIAA Lighter than Air Systems Conference, Clearwater, FL, AIAA Paper No. 95-1603-CP, 1995.

[7] Nagabhushan, B. L., and Tan, S. B., "Directional Control of An Advanced Airship," 11th AIAA Lighter than Air Systems Conference, Clearwater, FL, AIAA Paper No. 95-1626-CP, 1995.

[8] Khoury, G. H., and Gillett, J. D., (eds.), *Airship Technology*, Cambridge Univ. Press, Cambridge, England, U.K., 1999.

[9] Schmidt, D. K., Stevens, J., and Roney, J., "Near-Space Station Keeping Performance Of A Large High-Altitude Notional Airship," *Journal of Aircraft* (to be published); also, AIAA Atmospheric Flight Mechanics Conference, Keystone, CO, AIAA Paper No. 2006-6510, 2006.

[10] Anon., *Radionsonde Database Access* [online database], http://raob.fsl.noaa.gov [cited 15 Oct. 2005].

[11] Moorhouse, D., and Woodcock, R., "Background Information and User Guide for MIL-F-8785C, Military Specification: Flying Qualities of Piloted Airplanes," U.S. Air Force Wright Aeronautical Labs.. Rept. AFWAL-TR-81-3109, Wright–Patterson AFB, OH, July 1982.

[12] Swaim, R. L., Schmidt, D. K., Roberts, P. A., and Hinsdale, A. J., "An Analytical Method for Ride Quality of Flexible Airplanes," *AIAA Journal*, Vol. 15, No. 1, 1977.

[13] McLean, D., *Automatic Flight Control Systems*, Prentice–Hall, Upper Saddle River, NJ, 1990.